Direct VCSEL interconnection with a hollow core fiber

(Invited Paper)

Yongmin Jung[a,*], Jing Meng[a], Kerrianne Harrington[a,b], Hesham Sakr[a,c], Ian A. Davidson[a], Sijing Liang[a], Gregory Jasion, Francesco Poletti[a], and David J. Richardson[a,c]

[a] *Optoelectronics Research Centre, University of Southampton, Southampton SO17 1BJ, UK*

[b] *Now with Department of Physics, University of Bath, Claverton Down, Bath BA2 7AY, UK*

[c] *Now with Microsoft (Lumenisity), Unit 7, The Quadrangle, Abbey Park Industrial Estate, Romsey SO51 9DL, UK*

**Corresponding author: ymj@orc.soton.ac.uk*

The direct interconnection of a hollow-core fiber (HCF) to a laser diode or photodiode is essential to full exploitation of the unique characteristics of HCFs. In this paper, we investigate two specific methods for HCF interconnection (i.e., butt coupling and simple two-lens imaging) for coupling light from a single-mode vertical-cavity surface-emitting laser (VCSEL) operating at 850 nm. Our research findings indicate that direct (lensless) butt coupling leads to poor coupling efficiency (~10%) due to the significant mode field diameter (MFD) mismatch between the waveguide and the HCF. However, the efficiency can be significantly improved (up to approximately 69%) by using a graded-index fiber based all-fiber MFD converter. On the other hand, a two-lens system enables an extremely high coupling efficiency of ~96%.

Key Words: Hollow core fiber, interconnection, butt coupling, vertical-cavity surface-emitting laser (VCSEL), coupling efficiency, all-fiber MFD converter

1. Introduction

Hollow core fibers (HCFs) [1-3] have gained significant attention in recent years due to their distinctive optical properties, which include low optical loss, low non-linear effects, low glass-mode overlap, high optical damage threshold, and wide transmission bandwidth capable of covering regions that are difficult to access with solid core silica fibers. These remarkable features make them highly suitable for various applications such as optical communications, high power laser beam delivery, high-precision sensors, and Raman spectroscopy [4-7]. In particular, HCFs have the potential to revolutionize the telecommunication industry by supporting new low latency applications and the ability to deliver far more fiber capacity with wideband, low nonlinearity, low chromatic dispersion performance. Furthermore, HCF can transport high-power laser beams across a wide range of wavelengths, with recent demonstrations showing that HCF can handle kW continuous-wave lasers at 1.07 μm [4] and 14 mJ pulse energy at 2.94 μm [8]. However, to be useful in practical applications, it is necessary to develop reliable HCF interconnection techniques and the effective integration of HCF components. One of the primary challenges in HCF connectivity is reducing Fresnel reflection between solid core fiber and HCF, ensuring pure mode excitation in HCFs, and hermetically sealing the fiber without deforming the structure to maintain low loss at the interconnection. Recent advancements in micro-collimator technology have addressed some of these challenges and have demonstrated <1 dB fiber-to-fiber losses in micro-optic devices with ~10 mm air gaps. Additionally, an array of packaged isolator/filter devices have been created using this technology [9]. While these developments represent significant progress in HCF interconnectivity, further research is necessary to optimize HCF integration for practical applications.

One of the most important interconnection requirements concerns directly interfacing a HCF to a laser diode or photodiode as needed to fully exploit the unique characteristics of HCFs. While there has been extensive research on fiber coupled optical devices based on solid core fibers, there are only reports on the coupling of laser diodes and HCFs. In certain applications, even a short length of solid core fiber may not be suitable or cost-effective, particularly at extreme wavelengths such as in the ultraviolet (UV) or mid-infrared (mid-IR) spectral regions. HCFs have become increasingly popular at these wavelengths due to their low transmission loss and solarization-free UV transmission. Direct HCF interconnection, without any significant length of silica fiber, can enhance transmission stability and maintain beam quality. For instance, direct coupling between mid-IR quantum cascade lasers (QCLs) and HCFs may provide the easiest route to minimize the cost of a transmission cable, reduce losses and spurious reflections, and improve performance in mid-IR applications. Moreover, direct interconnection can be crucial in applications where ultimate latency is a key parameter, such as data center applications, where HCFs offer a solution to reducing latency and dispersion, while increasing spectral bandwidth and reach.

In this paper, we address the challenge of optical interconnection between VCSELs and HCFs, with a specific focus on two different methods: direct butt coupling and simple two-lens imaging. Through our investigations, we have gained valuable insights into the coupling characteristics between VCSEL and HCFs and demonstrated the

effectiveness of these two interconnection approaches. Our findings represent a significant contribution to the ongoing efforts to develop efficient, reliable, and cost-effective interconnection techniques for HCFs.

2. Direct fiber butt coupling between a VSCEL and an HCF

First, we focused on using fiber butt coupling as the simplest method for the VCSEL-HCF interconnection. This involves placing the end of the HCF in very close proximity to the emitter of a VCSEL, as illustrated in Fig. 1(a). Compared to traditional edge-emitting laser diodes (LDs), VCSELs offer several advantages. For instance, they provide excellent wavelength stability, making them relatively insensitive to temperature changes. Additionally, VCSELs exhibit exceptional beam circularity, rendering them well-suited for light coupling into optical fibers. In this context, we opted for a single-mode 850 nm VCSEL (LCV850SP2, Laser Components Ltd.) with a maximum output power of 1.4 mW and a well-defined Gaussian beam profile. This choice not only simplifies the experimental setup but also facilitates seamless coupling with HCFs. The VCSEL's divergence angle has been ascertained to be 22 degrees at $1/e^2$ intensity point, corresponding to a numerical aperture of ~0.19, while the spot size was estimated to be ~0.7 μm. Figure 1(b) depicts a microscope image captured from the top view of the VCSEL, which clearly shows the emitter emitting light perpendicular to the chip's surface, and a bond wire for electric connection situated about 75 μm away. Note that the VCSEL was initially packaged in a hermetic TO-46 can housing, but we removed the protective glass window for microscopic imaging and direct butt coupling experiments. A state-of-the-art HCF with nested anti-resonant nodeless fiber structure (NANF) [5] was employed in this demonstration. Fig. 1(c) shows a cross-sectional scanning electron microscope (SEM) image of the fiber. This HCF design incorporates six nested, anti-resonant capillaries within its cladding. This nested or multi-ring structure significantly enhance light confinement in comparison to a single-ring structure, and consequently enabling efficient light propagation with minimal losses, on the order of magnitude lower. The key physical dimensions of the HCF are as follows: an air-core diameter of 27 μm, a micro-structured cladding diameter of 75 μm, and an overall outer diameter of 204 μm. It is worth noting that these types of NANFs typically possess a relatively large core diameter, approximately 30 times the optical wavelengths. This characteristics results in a significant mode field diameter (MFD) of ~18.9 μm, which corresponds to ~70% of the core diameter. The average thickness of the glass membrane was ~470 nm, which is approximately half the wavelength of the light it operates with. This thickness is optimized for efficient light guidance within the second anti-reflection window centered at 850 nm. Rigorous simulations conducted using COMSOL software confirmed that the fundamental mode of the HCF presents a nearly Gaussian distribution, as illustrated in Fig. 1(d). Notably, the calculated beam profile closely aligns with a standard Gaussian beam, with an overlap factor of over 98%. The measured fiber loss was approximately 1.4 dB/km at 850 nm, which is lower than commercially available solid-core single-mode fibers (e.g., ~3.5 dB/km at 850 nm for 780HP). In our experiment, we used a total length of 1.04 km HCF.

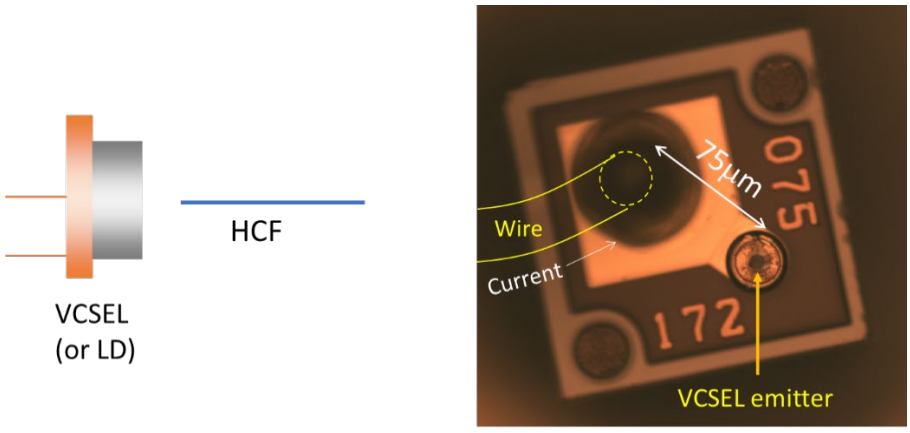

(a) (b)

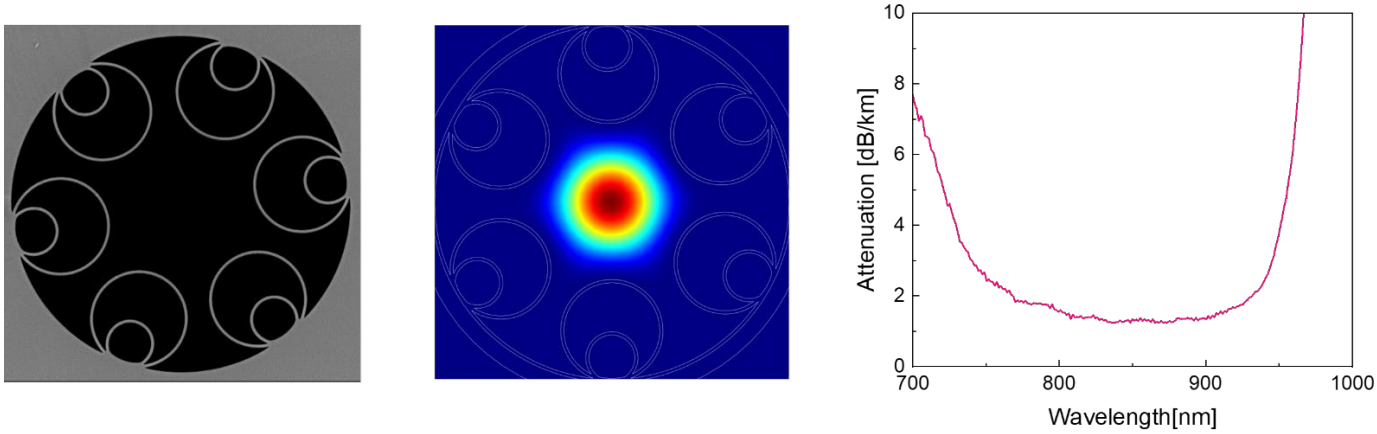

(c) (d) (e)

Fig. 1 (a) A schematic of the direct fiber butt coupling technique and (b) a microscope image of the VCSEL. (c) SEM image, (d) calculated fundamental mode, and (e) the attenuation characteristics of the HCF used in our experiment.

To begin with, the VCSEL was securely mounted onto a temperature-controlled laser mount, which was stabilized by a thermoelectric cooler (TEC) with the temperature set to around 20 degrees. The HCF was then flat-cleaved with an angle of less than 1 degree and positioned in a V-groove fiber holder that was mounted on a multi-axis stage to allow precise optical alignment. Using a microscope, we carefully aligned the VCSEL emitter and the fiber end, ensuring that they were in close proximity without making any physical contact. After achieving initial alignment, we used an optical power meter to finely adjust the alignment until maximum power output was reached in our butt coupling experiment. Despite our efforts, we were only able to achieve a coupling efficiency of approximately 10% at the optimized position. This low efficiency was mainly attributed to the significant MFD mismatch between the VCSEL chip and the HCF. It is important to note that the VCSEL waveguide's emitter dimension is typically sub-micron or micron-sized within the active layer, whereas the MFD of our HCF is around 18.9 μm at 850 nm, resulting in an order of magnitude difference in MFD between the two waveguides. Furthermore, the bond wire positioned approximately 75 μm away from the VCSEL emitter (as shown in Fig. 1(b)) hindered close access to the emitter due to the large outer diameter of the HCF (204 μm). To evaluate the axial displacement tolerance, we positioned the HCF at the point of maximum coupling efficiency with the VCSEL and then adjusted it in the axial direction. As shown in Fig. 3(a), the coupling loss decreased as the HCF was moved away from the emitter due to the increased MFD mismatch. We measured a 1 dB tolerance against axial displacement to be ~200 μm. Interestingly, relatively constant coupling efficiency was achieved at closer distances to the HCF, which we believe is related to the MFD mismatch and the beam divergence. This observation is currently under further investigation through simulation. To analyze the lateral offset tolerance, we conducted a two-dimensional (2D) scan of the HCF around the optimized position to obtain the power distribution [14]. We scanned the fiber over an area of 50 μm by 50 μm and sampled on a 100 by 100 step grid. As depicted in Fig. 2(b) the hexagonal shape of the HCF beam profile is evident due to the intensity overlap between the VCSEL chip and the HCF. The measured 1-dB lateral tolerance was approximately 13 μm. Our measurements show that the butt coupling of HCFs to VCSELs has relatively poor coupling efficiency but effectively larger tolerance to lateral and axial displacements compared to conventional solid-core single-mode fibers (SMFs).

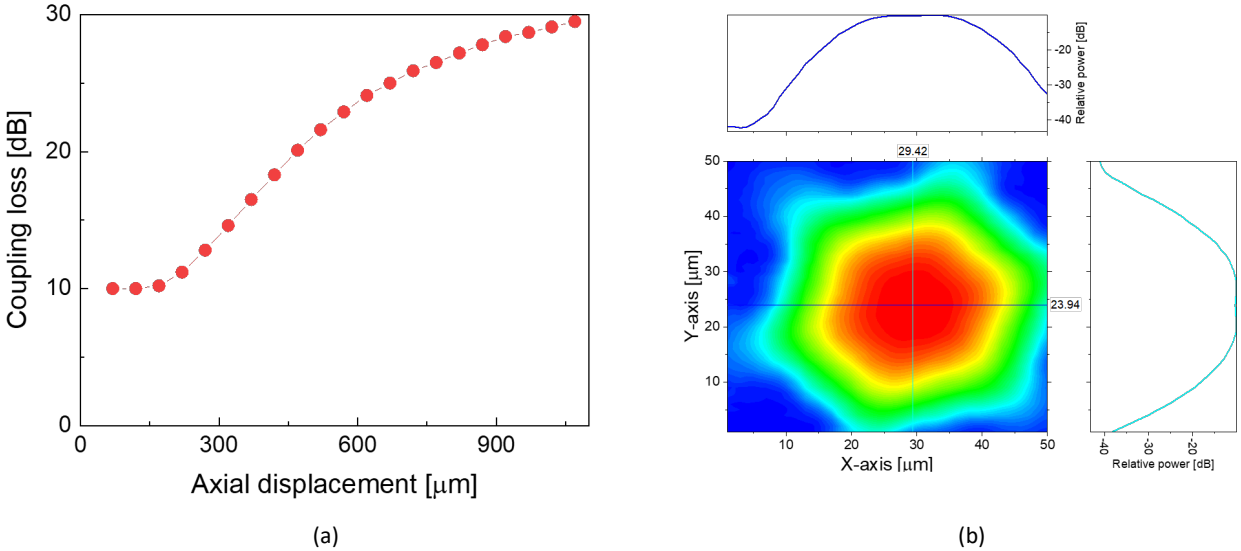

(a) (b)

Fig. 2 (a) Measured coupling loss according to the axial- and (b) lateral offset.

3. Enhanced fiber butt coupling using a graded-index fiber lens

To improve the efficiency of fiber butt coupling, we employed a graded-index fiber (GIF) lens element at the input end facet of the HCF as shown in Fig. 3(a). This technique involves using a single lens for image formation, and the size of the output plane image (in our case we are concerned with the beam MFD) can be adjusted by varying the magnification ratio of the object. Our design incorporates a GIF as a compact lens element in combination with a coreless fiber (CSF) segment serving as a spacer. By selecting the appropriate lengths of both fibers, a compact all-fiber MFD converter can be readily constructed using a simple cleaving and fusion splicing procedure. The GIF-lens-based all-fiber structure has previously been used to reduce splice loss between two dissimilar SMFs by adjusting their MFD mismatch [15], as well as for low-loss optical interconnection between dissimilar multicore fibers with different core pitch distances [16]. Initially, we performed simulations of the proposed fiber structure using the beam propagation method (BPM). We used a commercial OM4 graded-index multimode fiber with a 50 μm core diameter as the GIF and found that optimal fiber segment lengths for the GIF and CSF to maximize the coupling efficiency were 240 μm and 850 μm respectively. As depicted in Fig. 3(b), the divergent light from the VCSEL gradually converges after passing through the GIF, and the coupling efficiency gradually increases with an increase in CSF length. This enhancement in coupling efficiency is mainly due to the magnification process, which leads to an increased MFD at the image plane. With this method, approximately 90% coupling efficiency can be achieved in our simulation.

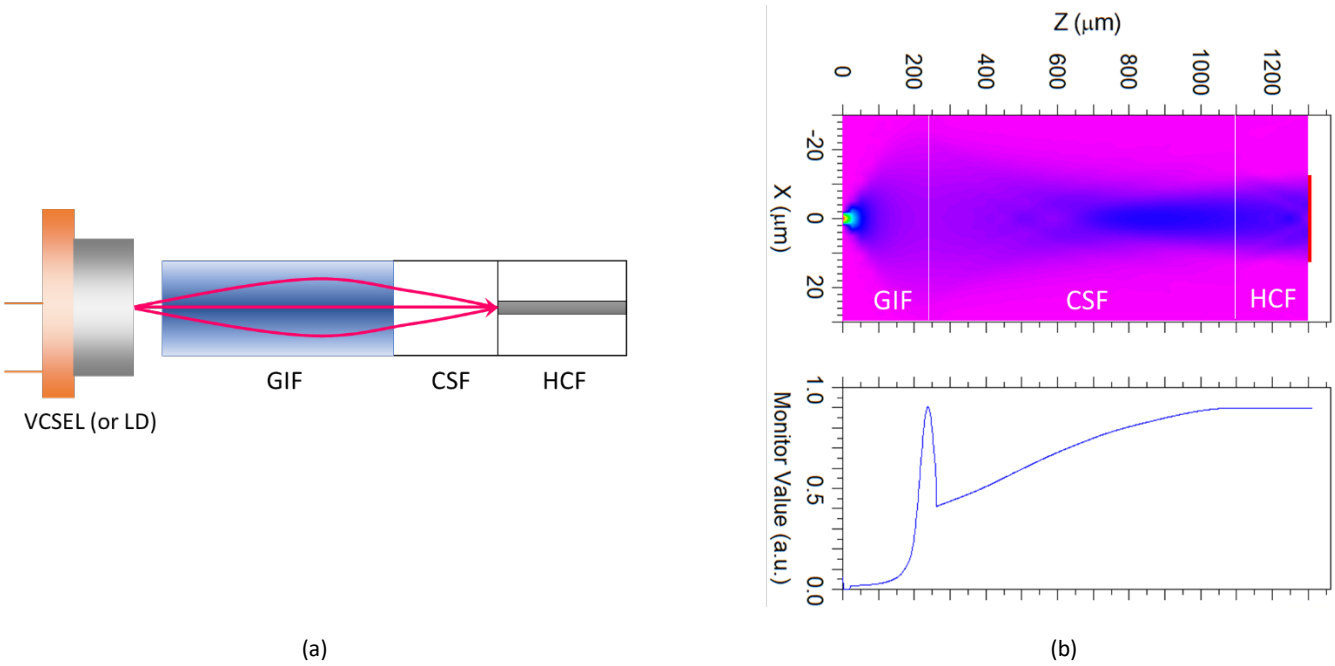

(a) (b)

Fig. 3 (a) A schematic of the graded-index fiber (GIF) enhanced fiber butt coupling and (b) BPM simulation.

To validate our simulation results, we fabricated an all-fiber MFD converter for efficient optical interconnection between a VCSEL and an HCF. The converter was created by splicing a 230 μm segment of GIF with a segment of CSF at the end facet of the HCF. To ensure accuracy and reliability, we used a high-precision cleaver in conjunction with a translation stage and a microscope to manipulate the fiber length [17]. During the fabrication process, we observed that the thin glass membranes of the HCF were susceptible to being distorted by the arc fusion during the CCF-HCF splice. To address this issue, we used a shorter CSF segment (700 μm instead of the initially planned 850 μm), assuming that the membrane collapse region is approximately 150 μm. It is worth noting that we considered this region of tube retraction to effectively provide additional spacing between the GIF and HCF. Figure 4(a) shows a microscope image of the fabricated MFD converter. The measured fiber segment lengths were 250 μm and 710 μm, respectively, demonstrating that our precision cleaver is capable of an accuracy of ~10 μm in terms of positioning. Using this MFD converter, we tested the fiber butt coupling efficiency and observed a substantial increase in coupling efficiency, reaching values as high as ~69% (1.61 dB loss). This improvement is approximately 7 times greater than what was achieved through direct HCF butt coupling. However, the observed coupling efficiency was slightly lower than the theoretical 90% value (0.45 dB loss) from simulation, which could be attributed to dopant diffusion within GIF and/or inaccurate assumptions regarding the length of microstructure collapse during the fiber fusion splice process. We believe that this can be further optimized in the future with better control of the fiber length and splice parameters. Using this all-fiber MFD converter, we tested the axial and lateral offset tolerance and found that the 1-dB alignment tolerance was reduced to 5 μm and 1.3 μm, respectively. This reduction is mainly due to the reduced MFD, which requires more careful active alignment of the HCF to minimize the coupling loss. In Fig. 4(c), a distinct stripe line can be observed in the 2D contour plot. This stripe is a result of the bond wire that was used for electric connection, located approximately 75 μm away from the emitter, which became visible when the fiber was scanned around the emitter.

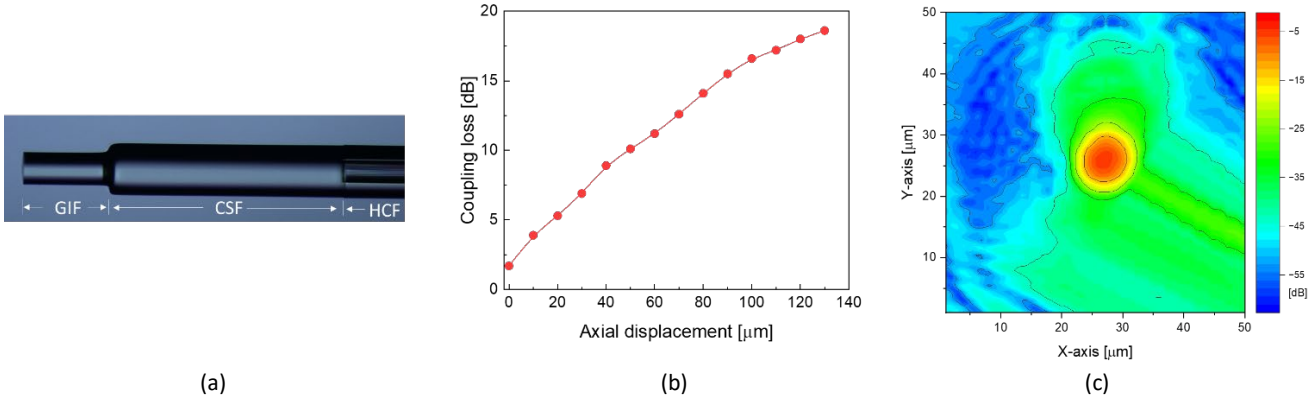

Fig. 4 (a) Microscope image of the fabricated all-fiber MFD converter consisting of a graded-index fiber and a coreless fiber. (b) Measured coupling loss according to the axial- and (c) lateral offset.

4. Simple two lens system

As an alternative approach to achieving direct interconnection between HCF and a VCSEL chip, a simple two-lens system was employed. This system effectively controls the mismatch in MFD by incorporating two lenses (L1 and L2 in Fig. 5(a)) to ensure optimal performance. The first lens (L1) with a short focal length is responsible for collimating the VCSEL beam. The second lens (L2) has a longer focal length and focuses the light into the HCF. The magnification ratio of the MFD is determined by the ratio of the focal lengths of the two lenses. We used the simulation tool Zemax to assist in the design of this two-lens system. In the simulation, we considered the HCF to be a simple step-index fiber with the same MFD at 850 nm to simplify the calculation of coupling efficiency. An aspheric lens with a short focal length (4.5 mm) was chosen as a collimator so that the magnification ratio can be varied practically over a wide range simply by changing the focal length of L2, which allowed us to search for the optimum L2. Figure 5(b) shows the calculated coupling efficiency as a function of the focal length of L2, represented by the black line with circular data points. The simulation results indicate that a focal length of 26 mm is optimal for coupling into the fundamental mode of the HCF, with a maximum coupling efficiency of approximately 98%. Notably, even for slight focal length offset of L2, coupling efficiency remains impressive, consistently surpassing >95% within the focal length range of 23.7 mm to 30.5 mm. It was observed that shorter focal lengths incur a faster increase in coupling loss compared to longer focal lengths. To validate the simulation results, an experiment was conducted to test the performance of various focal lengths of L2. The measurements are shown in Fig. 5(b) with the red line with square data points. The general trend observed in the experiment was quite similar to that observed in the simulation. Specifically, when using an L2 focal length of 18.4 mm, the coupling efficiency reached a maximum of around 96%, which aligns closely with the theoretical estimates. Furthermore, after the light propagated through 1.04 km of HCF, the presence of a clean fundamental mode was confirmed by analyzing the far-field beam profile of the light, as shown in the inset figure in Fig. 5(b).

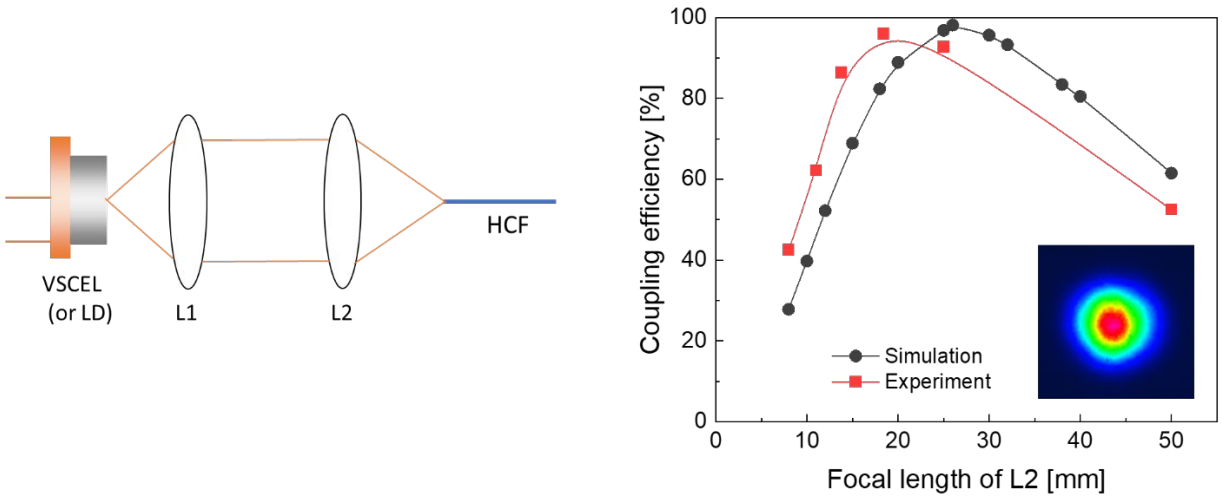

(a) (b)

Fig. 5 (a) A schematic of a simple two-lens system and (b) simulation and experimental coupling efficiency results according to the choice of lens L2.

5. Conclusions

Our investigation focused on the optical interconnection between VCSEL and hollow core fiber, specifically on two HCF interconnection methods: direct butt coupling and simple two-lens imaging. Our results indicate that simple direct butt coupling (i.e. without any lenses) provides poor coupling efficiency (~10%) due to the significant mode field diameter mismatch. However, we were able to improve the coupling efficiency to ~69% by using an all-fiber MFD converter based on a graded-index fiber lens, which is broadly consistent with the coupling efficiency of 90% from simulation. We also explored the use of a two-lens systems, which proved highly effective, achieving a coupling efficiency of ~96% with an appropriate lens combination. Our future work will involve investigating the coupling of other semiconductor lasers to HCFs across various wavelength bands, particularly mid-IR QCLs and visible/UV laser diodes.

Acknowledgements

This work was supported in part by the EPSRC funded “Airguide Photonics” Programme Grant (EP/P030181/1) and “National Hub in High Value Photonics Manufacturing” (EP/N00762X/1). For the purpose of open access, the authors have applied Creative Commons Attribution (CC BY) license to any Accepted manuscript version arising from this submission and all data supporting this study are openly available from the University of Southampton repository at http://doi.org/10.5258/SOTON/D2755.

References

[1] R. Cregan, B. Mangan, J. Knight, T. Birks, P. S. J. Russel, P. Roberts, and D. Allan, Single-mode photonic band gap guidance of light in air, Science 285 (1999), 1537-1539.
[2] P. Russell, Photonic crystal fibers, Science 299 (2003), 358-362.
[3] F. Poletti, N. Wheeler, M. Petrovich, N. Baddela, E. N. Fokoua, J. Hayes, D. Gray, Z. Li, R. Slavík, and D. J. Richardson, Towards high-capacity fibre-optic communications at the speed of light in vacuum, Nat. Photonics 7 (2013), 279-284.
[4] H. C. H. Mulvad, S. Abokhamis Mousavi, V. Zuba, L. Xu, H. Sakr, T. D. Bradley, J. R. Hayes, G. T. Jasion, E. Numkam Fokoua, A. Taranta, S. -U. Alam, D. J. Richardson, and F. Poletti, Kilowatt-average-power single-mode laser light transmission over kilometre-scale hollow core fibre, Nat. Photonics 16, (2022) 448-453.
[5] F. Benabid, J. C. Knight, G. Antonopoulos, P. St. J. Russell, “Stimulated Raman scattering in hydrogen-filled hollow-core photonic crystal fiber,” Science 298, 399-402 (2002).
[6] P. St. J. Russel, P. Holzer, W. Chang, A. Abdolvand and J. C. Travers, “Hollow-core photonic crystal fibres for gas-based nonlinear optics,” Nat. Photonics 8, 278-286 (2014).
[7] R. Slavik, G. Marra, E. N. Fokoua, N. Baddela, N. V. Wheeler, M. Petrovich, F. Poletti, and D. J. Richardson, Ultralow thermal sensitivity of phase and propagation delay in hollow core optical fibres, Sci. Reports 5 (2015), 15447.

[8] A. Urich, R. R. Maier, B. J. Mangan, S. Renshaw, J. C. Knight, D. P. Hand, and J. D. Shephard, Delivery of high energy Er:YAG pulsed laser light at 2.94 μm through a silica hollow core photonic crystal fibre, Opt. Express 20 (2012), 6677-6684.
[9] Y. Jung, H. Kim, Y. Chen, T. D. Bradley, I. A. Davidson, J. R. Hayes, G. Jasion, H. Sakr, S. Rikimi, F. Poletti, and D. J. Richardson, Compact micro-optic based components for hollow core fibers, Opt. Express 28 (2020),1518-1525.
[10] K. Pierściński, G. Stępniewski, M. Klimczak, G. Sobczak, D. Dobrakowski, D. Pierścińska, D. Pysz, M. Bugajski, and R. Buczyński, Butt-coupling of 4.5 μm quantum cascade lasers to silica hollow core anti-resonant fibers, J. Lightwave Technol. 39 (2021) 3284-3290.
[11] B. Siwicki, R. M. Carter, J. D. Shephard, F. Yu, J. C. Knight, D. P. Hand, Negative-curvature anti-resonant fiber coupling tolerance, J. Lightwave Technol. 37 (2019), 5548-5554.
[12] G. S. Kliros and G. K. Paschalidis, Calculation of coupling losses between laser diodes and large mode area photonic crystal fibers, 2016 International Workshop on Fiber Optics in Access Network (FOAN), Lisbon, Portugal, 2016, pp. 1-6, doi: 10.1109/FOAN.2016.7764546.
[13] H. Sakr, Y. Chen, G. T. Jasion, T. D. Bradley, J. R. Hayes, H. C. H. Mulvad, I. A. Davidson, E. N. Fokoua, F. Poletti, Hollow core optical fibres with comparable attenuation to silica fibres between 600 and 1100 nm, Nat. Communications 11 (2020), 6030.
[14] Y. Jung, A. Wood, S. Jain, Y. Sasaki, S.-U. Alam, and D. J. Richardson, Fully integrated optical isolators for space division multiplexed (SDM) transmission, APL Photonics 4 (2019), 022801.
[15] P. Hofmann, A. Mafi, C. Jollivet, T. Tiess, N. Peyghambarian and A. Schülzgen, Detailed investigation of mode-field adapters utilizing multimode-interference in graded index fibers, J. Lightwave Technol. 30 (2012), 2289-2298.
[16] Y. Jung, J. R. Hayes, Y. Sasaki, K. Aikawa, S. U. Alam, and D. J. Richardson, All-fiber optical interconnection for dissimilar multicore fibers with low insertion loss, in Optical Fiber Communication conference (Optica Publication Group, 2017), paper W3H.2., https://doi.org/10.1364/OFC.2017.W3H.2
[17] Y. Jung, S. Lee, B. H. Lee, and K. Oh, Ultracompact in-line broadband Mach-Zehnder interferometer using a composite leaky hollow-optical-fiber waveguide, Opt. Letters 33 (2008), 2934-2936.